Mon. Not. R. Astron. Soc. **000**, 000–000 (0000) Printed 19 January 2019 (MN LATEX style file v1.4)

Photon Scattering by Relativistic Flows in Schwarzschild Spacetimes. I. The Generation of Power-Law Spectra

Hara Papathanassiou[1], Dimitrios Psaltis[2,3]

[1] *International School for Advanced Studies (SISSA), Via Beirut 2-4, 34013 Trieste, Italy*
[2] *Center for Space Research, Massachusetts Institute of Technology, Cambridge, MA 02139, U.S.A.*
[3] *Harvard-Smithsonian Center for Astrophysics, 60 Garden St., Cambridge, MA 02138, U.S.A.*

19 January 2019

ABSTRACT

We study the spectra generated as a result of bulk Comptonization by relativistic electrons in radial flows onto compact objects. We solve numerically the general-relativistic radiative transfer equation in the Schwarzschild spacetime, in steady-state and under minimal assumptions. We show that power-law spectra result from multiple scatterings, in a way similar to thermal Comptonization. We also find that photon-electron interactions taking place near the black-hole event horizon affect very little the emerging spectra. We, therefore, argue that bulk Comptonization spectra do not carry distinguishing signatures of the compact object around which they are produced. We examine the dependence of the spectra on simplifications often employed regarding the spacetime geometry, the distribution of photon sources, and the boundary conditions. We show that the existence of trapped characteristics around a black hole reduces the efficiency of Comptonization and that general relativistic effects identically cancel bulk Comptonization effects for a free-falling flow and in the limit of infinitesimal mean-free path. As a result, we find that neglecting the curved spacetime geometry leads to overestimating the high-energy flux by up to an order of magnitude. Finally, we demonstrate that the spectrum from accretion onto a neutron star depends sensitively on the imposed boundary conditions, while that from a black hole is immune to such choices.

Key words: accretion – black hole physics – radiation mechanisms: non-thermal – radiative transfer – methods: numerical – stars: neutron

1 INTRODUCTION

Compton scattering of photons in media with non-negligible bulk velocities is thought to be a significant, or even the dominant, radiative process in a number of astrophysical settings. Examples include the early Universe (the kinematic Sunyaev-Zeldovich effect; see, e.g., Rephaeli 1995), jets in blazars (see, e.g., Sikora, Begelman & Rees 1994), gamma-ray bursts (see, e.g., Lazzati et al. 2000; Madau & Thompson 2000), and accretion flows onto galactic compact objects (see, e.g., Payne & Blandford 1981). The interaction of neutrinos with fast-moving electrons is also thought to determine the dynamics and fate of supernova explosions and super-critical accretion flows onto neutron stars (see, e.g., Fryer, Benz & Herant 1996; Burrows et al. 2000).

Studying any of the above problems requires the solution of the kinetic equation that describes scattering of massless particles by fast-moving electrons, in which relativistic effects introduce very strong angular and photon-energy dependences. Because of such complexities, most previous studies have made a number of approximations in treating this radiative transfer problem (see Psaltis & Lamb 1997 and references therein). The kinetic equation is often expanded to different orders in the electron bulk velocity β (in units of the speed of light) and/or the photon energy $\epsilon/m_{\rm e}$ (where $m_{\rm e}$ is the electron rest mass) and is truncated keeping only terms up to a low order (Blandford & Payne 1981; Mastichiadis & Kylafis 1992; Titarchuk, Mastichiadis & Kylafis 1997). Furthermore, general relativistic effects are most usually neglected (but see Schmid–Burgk 1978; Zane et al. 1996; Titarchuk & Zannias 1998; Laurent & Titarchuk 1999). Such analyses show that the effects of the odd- and even-order terms in β are qualitatively and quantitatively different and their relative importance is determined not only by the magnitude of the bulk velocity but by the properties of the radiation field and the flow as well (Psaltis & Lamb 1997, 2000).

The configuration in which Compton scattering of photons by relativistic electrons has been studied extensively

in the past is that of accretion flows onto compact objects. Recent motivation for such studies comes from the observed power-law shapes and the absence of any detectable cut-offs (up to energies comparable to the rest mass of the electron) in the γ-ray spectra of galactic accreting black holes (Grove et al. 1998). Attributing these spectra to Comptonization by the relativistic electrons in the accretion flow could provide a spectral signature for the existence of a black hole in a galactic system and even lead to the measurement of its mass (as suggested in, e.g., Chakrabarti & Titarchuk 1996; Shrader & Titarchuk 1998, 1999; Laurent & Titarchuk 1999; Borozdin et al. 1999).

Various analytical (Payne & Blandford 1981; Mastichiadis & Kylafis 1992; Turolla et al. 1996; Titarchuk & Zannias 1998; Zampieri & Lamb 2000) and numerical (Zane et al. 1996; Titarchuk et al. 1997; Laurent & Titarchuk 1999; Psaltis 2000) treatments have been employed in previous studies of bulk Comptonization. However, the results of several analytic solutions have been recently questioned because of the inadequate order to which the transfer equations was truncated (see discussion in Psaltis & Lamb 1997, 2000) or of the inappropriate mathematical methods employed (see discussion in Zampieri & Lamb 2000). Moreover, previous numerical studies have either considered a limited number of cases (as in, e.g., Zane et al. 1996) or used approximate treatments which severely affected the properties of the solutions (see discussion in Psaltis & Lamb 2000).

With this paper we initiate a study of Compton scattering in relativistic accretion flows and winds, performed under a minimal set of assumptions and approximations, in order to address a number of questions that previous treatments raised. We solve numerically the kinetic equation for massless particles in a Schwarzschild spacetime derived by Lindquist (1966), using an iterative integration along the curved photon characteristics (Schmid–Burgk 1978; Zane et al. 1996). In this first study, we investigate the effects on the emerging spectra of properties related to the flow velocity, the metric, the boundary conditions, and the distribution of sources in the flow. We only assume that the systematic down-scattering of photons as well as the Klein–Nishina corrections to the scattering cross section (which are of the same order) are negligible. Therefore, we cannot address issues related to the high-energy cut-offs of the spectra and their shapes at photon energies comparable to, or higher, than the electron rest mass; we will discuss these elsewhere.

2 RADIATIVE TRANSFER IN A SCHWARZSCHILD SPACETIME

Throughout this paper we use geometric units ($c = G = 1$) and describe the radiation field in terms of the photon occupation number $f(r, \mu, \epsilon)$. We assume that the spacetime is static and spherically symmetric and, therefore, the occupation number depends only on the radius r (hereafter normalised to $2M$, where M is the mass of the central object), the cosine μ of the angle between the radial direction and the photon propagation vector, and the photon energy ϵ appropriately normalised and measured in the local rest frame. We define the necessary moments of the photon field

$$J(r,\epsilon) \equiv \frac{1}{2}\int_{-1}^{1} f(r,\mu,\epsilon)\epsilon^3 d\mu \,, \tag{1}$$

$$H(r,\epsilon) \equiv \frac{1}{2}\int_{-1}^{1} f(r,\mu,\epsilon)\epsilon^3 \mu d\mu \,, \tag{2}$$

$$K(r,\epsilon) \equiv \frac{1}{2}\int_{-1}^{1} f(r,\mu,\epsilon)\epsilon^3 \mu^2 d\mu \,, \tag{3}$$

so that the energy flux emerging from the flow, which will be the primary quantity of interest, is

$$F(\epsilon) = 4\pi \lim_{r\to\infty} H(r,\epsilon) \,. \tag{4}$$

In what follows, we assume $\epsilon \ll m_{\rm e}$ and neglect any polarisation-dependent effects. The steady-state photon kinetic equation for the photon occupation number in a spherically symmetric spacetime is (Lindquist 1966)

$$\begin{aligned} \sqrt{-g_{oo}}\gamma(\mu+\beta)\frac{\partial f}{\partial r} &+ \\ \sqrt{-g_{oo}}\gamma(1-\mu^2)\left[\frac{1+\beta\mu}{r} + g_{oo}\gamma^2(\mu+\beta)\frac{\partial\beta}{\partial r}\right]\frac{\partial f}{\partial \mu} &- \\ \sqrt{-g_{oo}}\gamma\left[\frac{\beta(1-\mu^2)}{r} - g_{oo}\gamma^2\mu(\mu+\beta)\frac{\partial\beta}{\partial r}\right]\epsilon\frac{\partial f}{\partial\epsilon} &= \\ \frac{\eta(r,\epsilon)}{\epsilon^3} - \chi(r,\epsilon) f \,, \end{aligned} \tag{5}$$

where $\gamma \equiv (1-\beta^2)^{-1/2}$ is the Lorenz factor, $g_{oo} = -(1-1/r)$ for Schwarzschild geometry, and $g_{oo} = -1$ for flat geometry. In the limit $\epsilon \ll m_{\rm e}$, we include the effects of scattering by setting

$$\chi(r,\epsilon) = \chi_{\rm a}(r,\epsilon) + n_{\rm e}(r)\sigma_{\rm T} \tag{6}$$

and

$$\begin{aligned} \eta(r,\epsilon) = \eta_{\rm e}(r,\epsilon) + \frac{3}{8} n_{\rm e}\sigma_{\rm T}\left[\left(3-\mu^2\right)J(r,\epsilon)\right. \\ \left. + \left(3\mu^2-1\right)K(r,\epsilon)\right] \,, \end{aligned} \tag{7}$$

where $\eta_{\rm e}(r,\epsilon)$ and $\chi_{\rm a}(r,\epsilon)$ are the emission and absorption coefficients, $\sigma_{\rm T}$ is the Thomson scattering cross section, and $n_{\rm e}(r)$ is the electron number density, all evaluated in the local rest frame. By writing f as a full differential of the path length s along each photon ray, Eq. [5] simplifies to (see Schmid–Burgk 1978 and Zane et al. 1996 for the details of the method which we summarise here for completeness)

$$\frac{df}{ds} = \frac{\eta}{\epsilon^3} - \chi f \,, \tag{8}$$

where

$$\frac{dr}{ds} = \sqrt{-g_{oo}}\gamma(\mu+\beta) \tag{9}$$

$$\frac{d\mu}{ds} = \sqrt{-g_{oo}}\gamma(1-\mu^2)\left[\frac{1+\beta\mu}{r} + g_{oo}\gamma^2(\mu+\beta)\frac{\partial\beta}{\partial r}\right] \tag{10}$$

$$\frac{d\epsilon}{ds} = \sqrt{-g_{oo}}\gamma\left[\frac{\beta(1-\mu^2)}{r} - g_{oo}\gamma^2\mu(\mu+\beta)\frac{\partial\beta}{\partial r}\right]\epsilon \,. \tag{11}$$

Algebraic manipulation of Eqs. [8]–[11] results in the simple ordinary differential equation (Zane et al. 1996)

$$\frac{df}{dr} = \frac{\eta/\epsilon^3 - \chi f}{\sqrt{-g_{oo}}\gamma(\mu+\beta)} \,, \tag{12}$$

where

$$\mu = \frac{g_{oo}b^2\beta\gamma^2 \pm r\sqrt{r^2 + g_{oo}b^2}}{r^2 - g_{oo}b^2\beta^2\gamma^2} \,, \tag{13}$$

$$\epsilon = \frac{\epsilon_\infty}{\sqrt{-g_{oo}}\gamma(1+\beta\mu)} \,. \tag{14}$$

The two last expressions make use of the two quantities that are conserved along a characteristic; the impact parameter b, and the photon frequency as measured at infinity ϵ_∞. Characteristics with $b \leq \sqrt{r_{\rm in}/|g_{oo}|}$ connect the inner boundary $r_{\rm in}$ with infinity. In the Schwarzschild geometry, for every impact parameter with $b > 3\sqrt{3}/2$, there exists one characteristic curve that reaches infinity and one that is trapped in the region $r < 1.5$. The trajectory with $b = 3\sqrt{3}/2$ has a critical saddle point at radius $r = 1.5$ and is a circle with this radius.

We use different boundary conditions depending on the type of the characteristics. For the ones that reach infinity, we integrate from the outer boundary along an incoming ray ($\mu < 0$, using the negative-sign branch of solution [13]), setting appropriate boundary conditions for no external illumination, i.e., $f(r_{\rm out}, \mu < 0, \epsilon) = 0$. For non-trapped characteristics that do not intersect the central object, the turning points are reached when $\mu = -\beta$ and the solution for μ simply switches to the positive-sign branch of Eq. [13]. For characteristics that reach infinity but do intersect the central object, we impose an additional boundary condition at $r_{\rm in}$, which depends on the problem under consideration. Typically, for the case of a neutron star, we set $f(r_{\rm in}, \mu > 0, \epsilon) = [1 - \exp(-\epsilon/T_{\rm b})]^{-1}$, i.e., a blackbody of temperature $T_{\rm b}$, whereas for a black hole, we set $f(r_{\rm in}, \mu > 0, \epsilon) = 0$, i.e., no illumination. Finally, we use similar boundary conditions for the trapped characteristics. When including photon sources in the flow, the emissivity η needs to be specified in Eq. [12], in addition to the terms that describe scattering. In the idealised problems considered here, we use two different photon sources that mimic more realistic models of accretion flows. First, in order to model the effects of volume emission, we adopt a blackbody source of photons of constant temperature and an emission measure that is proportional to a power of the electron density. Second, in order to model the effects of a soft-photon input from an underlying accretion disk, we adopt a blackbody source of photons with an emission measure proportional to the viscous dissipation rate in an accretion disk, such that the blackbody temperature at each radius is given by the standard thin-disk solution (Shakura & Sunyaev 1973)

$$T(r) = \begin{cases} T_{\rm in} \left(\frac{3}{r}\right)^{3/4} \left(1 - \sqrt{\frac{3}{r}}\right)^{1/4}, & \text{for} \quad r \geq 3 \\ 0\,, & \text{for} \quad r < 3, \end{cases} \tag{15}$$

where $T_{\rm in}$ is the temperature at $r = 3$, inside which the accretion disk is assumed to be an inefficient source of photons. Note here that the photon-energy scale in our solutions is specified only by the boundary conditions or the photon sources, since we have assumed $\epsilon \ll m_{\rm e}$. As a result, in all calculations the photon energy is normalised to the blackbody temperature of the illuminating boundary (for some neutron-star cases), the temperature of the photon sources within the flow, or $T_{\rm in}$ (when a disk-like emissivity is assumed).

Finally, we typically set the electron velocity and density profiles in the flow to their free-fall values, i.e., $\beta = -r^{-1/2}$ and $n_e \sim r^{-3/2}$, and specify the normalisation of the latter through the quantity

$$\tau(r) \equiv \int_r^{r_{\rm out}} n_e(r) \sigma_{\rm T} dr \tag{16}$$

evaluated at $r_{\rm in}$ which we call the optical depth. This is related to other quantities often used in describing such flows (Psaltis & Lamb 1997). One such example is

$$t_{\rm V}(r) \equiv -3 n_e(r) \sigma_{\rm T} \beta(r) r = \frac{3}{2} \frac{\tau(r)}{\sqrt{r}}\,, \tag{17}$$

which is equal to unity at the so-called photon trapping radius[⋆]. Another is

$$\frac{\dot{M}}{\dot{M}_{\rm E}} = \left(\frac{L}{\dot{M}}\right) r_{\rm in}^{1/2} \tau(r_{\rm in})\,, \tag{18}$$

the mass accretion rate measured at infinity, in units of the Eddington critical accretion rate (at which the outward radiation force balances gravity) of an accretion flow that produces luminosity L with an efficiency $L/\dot{M}$. Note, that when the accretion rate becomes comparable to the Eddington critical rate, the assumption of a free-fall velocity and density profiles is not justified, as the outward radiation force on the accreting gas becomes non-negligible.

3 NUMERICAL METHOD

We integrate Eq. [12] for a given impact parameter and photon energy (as measured by an observer at infinity) by a 4-th order Runge–Kutta method. We use, in most cases, a logarithmically equidistant grid in radius r between the inner boundary $r_{\rm in}$, which depends on the particular problem, and the outer boundary $r_{\rm out}$ representing infinity. We fix the value of $r_{\rm out}$ to 30. For the case of a neutron star we set $r_{\rm in} = 2.5$, while for that of a black hole $r_{\rm in} = 1.01$, to avoid the coordinate singularity at the event horizon. When modelling a scattering problem of high optical depth around a black hole, we use, instead, a grid that is logarithmically equidistant in $r - 1$. This choice of the r grid allows us to reach arbitrarily close to the black hole event horizon and with very fine resolution. This is necessary in order to deal with the very steep derivatives present near the event horizon. Our grid in the impact parameter b is built with two different spacing prescriptions (Zane et al. 1996). For $0 \leq b \leq \sqrt{r_*/|g_{oo}(r_*)|}$, where $r_* \equiv \max\{{\rm r_{in}}, 1.5\}$, we use

$$b_j = \frac{r_*}{\gamma(r_*)\sqrt{-g_{oo}(r_*)}} \frac{\sqrt{1-\mu_j^2}}{1+\beta(r_*)\mu_j}\,, \tag{19}$$

with

$$\mu_j = -1 + (j-1)\frac{2}{N-1} \tag{20}$$

for the $j-$th point, which guarantees N (usually 20) points spaced equally in μ at r_*[†]. For $\sqrt{r_*/|g_{oo}(r_*)|} < b \leq r_{\rm out}$, the grid on b is constructed according to the method of tangent rays, i.e., so that the turning point ($r_{\rm min} = \sqrt{-b^2 g_{oo}}$) of each characteristic lies very close to an r grid point.

⋆ This is the radius below which photons are advected inwards by the flow more efficiently than they are diffused outwards by scattering. It is not associated with the existence of trapped characteristics which are defined in §3.

† Choosing $r_* = 1.5$ instead of $r_{\rm in}$, for the black-hole case, provides better angular sampling around $r = 1.5$ which would otherwise create an artificial spiky feature in the radial profiles of the various radiation quantities.

For the photon energy grid we use an equidistant logarithmic grid that covers the range of the comoving energies we want to calculate the radiative processes in. We fix the range from $\epsilon_{\rm min} = 0.1$ to $\epsilon_{\rm max} = 500$ (in units of the black-body temperature of the photon source or the illuminating inner boundary). The gravitational and Doppler shifts experienced by the photons as they propagate through the flow will cause radiation that is produced locally in the above spectral range to appear at the observer in a much wider range; of course, this range depends on the compactness of the central object and is much wider for a black hole than for a neutron star. For example, if we place the inner boundary at $r_{\rm in} = 1 + \delta r$, with $\delta r \ll 1$, photons with locally measured energy ϵ in the $[\epsilon_{\rm min}, \epsilon_{\rm max}]$ interval will appear at the observer with an energy ϵ_∞ in the range

$$\epsilon_{\infty,{\rm min}} = \frac{\delta r}{2}\epsilon_{\rm min} \leq \epsilon_\infty \leq 2\epsilon_{\rm max} = \epsilon_{\infty,{\rm max}} \qquad (21)$$

(see Eq. [14]). For this reason, we maintain a logarithmic grid for $\epsilon_{\rm min} \leq \epsilon \leq 2\epsilon_{\rm max}$ and add a fixed number of logarithmically (but more sparsely) spaced points to cover energies below $\epsilon_{\rm min}$.

As in all scattering problems, Eq. [12] is an integro-differential equation and can, therefore, be most easily solved by an iterative procedure. In all our calculations we neglect true absorption and confine our attention to configurations with scattering optical depths of order unity. It is, therefore, adequate to use a simple variant of the $\Lambda-$iteration method (Mihalas 1978), which typically converges after a few iterations. We have validated the implementation of the numerical algorithm by comparing our solutions to simple analytical results derived in appropriate limits and to the numerical results reported for flat spacetimes and small electron velocities in Psaltis (2000).

4 RESULTS FOR NEUTRON STARS

We first model the transport of photons in an accretion flow that contains no photon sources but is illuminated from its inner boundary. This configuration allows us to study the effects on the spectrum of the propagation of photons through a relativistic medium, independent of the potential complication introduced by the radial profiles of sources (cf. Psaltis & Lamb 2000). Although idealised, our calculations are applicable to cold radial accretion flows onto neutron stars, if most of the accretion luminosity is released at the impact of the flow with the stellar surface.

Fig. 1 shows the spectra emerging from such a flow for different optical depths. The results of the calculation presented in this figure provide additional support to the suggestion that the generation of a power-law high energy spectrum is a general feature of Comptonization by relativistic inflows (see, e.g., Payne & Blandford 1981; note, however, that all early papers neglected the terms that describe the effect we discuss here).

The physical reason behind the generation of the power-law spectral tails is not readily obvious. For example, in the limit of very small optical depth, very few photons interact with electrons more than once and, therefore, it might appear reasonable to use a single-scattering approximation in calculating the emerging spectrum. If this were the case,

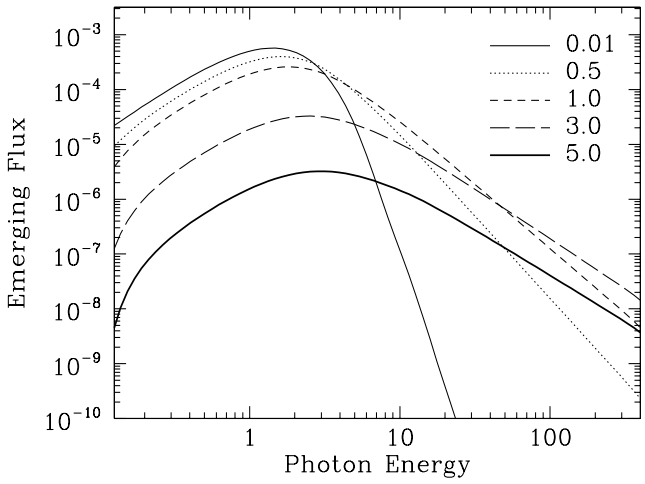

Figure 1. Radiation spectra emerging from radial accretion flows onto a neutron star for representative optical depths. The flows are illuminated at their inner boundary by the same black-body spectrum. The emerging flux is in arbitrary units and the photon energy is in units of the temperature of the illuminating black-body spectrum.

different photons interacting with electrons of different velocities would gain different amounts of energy and, since the electrons in the flow have a power-law velocity profile, they would potentially generate a power-law spectral tail. The result would then be equivalent to the generation of a power-law spectrum produced in optically thin, non-thermal plasmas, when low-energy photons are scattered once by electrons with a power-law velocity distribution (Coppi 1999). On the other hand, the distribution of photon escape times in the flow has an exponential tail at late times and this, convolved with an exponential increase of photon energy per scattering, can also produce a power-law high-energy tail as a result of multiple scatterings (as suggested by the Monte-Carlo simulations of Laurent & Titarchuk (1999)). This would be similar to the generation of power-law spectral tails in media that are optically thick to (either thermal or non-thermal) Comptonization (Sunyaev & Titarchuk 1980; Coppi 1999).

We can address the aforementioned question by calculating separately the spectra of photons that emerge from a flow after having interacted with electrons a given number of times. For this purpose, we decompose the radiative transfer equation (12) into a system of equations for the individual scattering orders as

$$\sqrt{-g_{oo}}\gamma(\mu+\beta)\frac{df_n}{dr} = \frac{\eta_{n-1}}{\epsilon^3} - \chi f_n \ , \qquad (22)$$

where $n = 1, 2,...$ represents the scattering order. We solve Eq. [22] for the zeroth order setting $\eta_{-1} = 0$ and using the same boundary conditions as in the full problem, i.e., illumination from the inner boundary. We then solve the same equation for each successive order n, calculating η_{n-1} from the solution of the previous order (through Eq. [7],) and setting the appropriate boundary conditions for a medium that is not illuminated from either boundary.

Fig. 2 shows the decomposition into scattering orders of the energy spectra emerging from two flows with different optical depths. In both cases, the spectrum calculated for

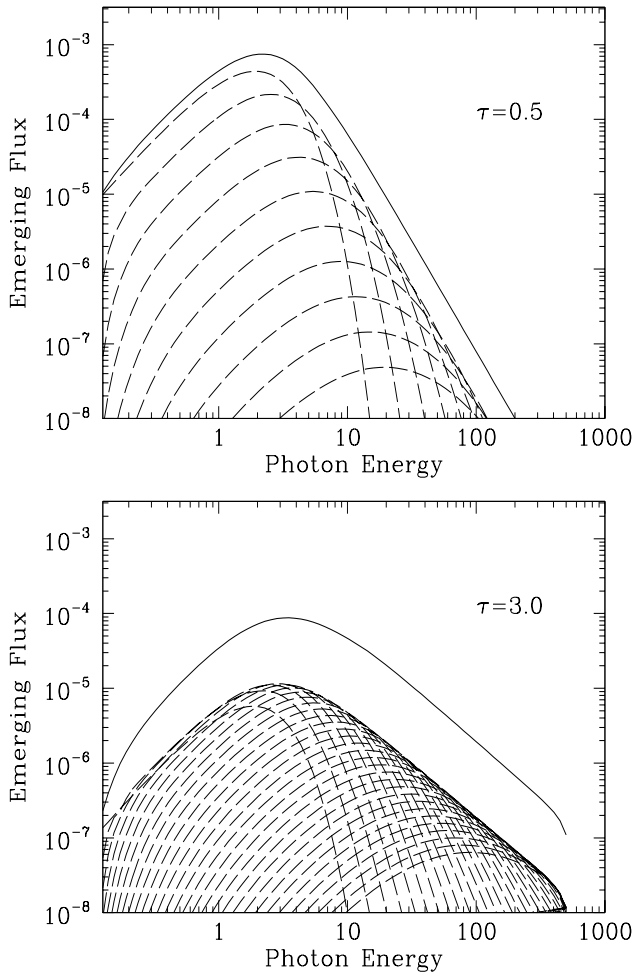

Figure 2. Decomposition into scattering orders (dashed lines) of the energy spectra (solid lines) emerging from two of the accretion flows presented in Fig. 1. The leftmost dashed line corresponds to the zeroth scattering order, i.e., the photons that reached the observer without having interacted with electrons. Each subsequent dashed line to its right corresponds to an increasingly higher scattering order.

each scattering order is displaced and broadened compared to the spectrum of the previous order while the fractional change of the mean photon energy is comparable to an average value of β^2 in the flow. This is demonstrated in Fig. 3, where the mean energy of photons emerging after each successive scattering order, defined as

$$\langle\epsilon\rangle_n = \frac{\int_0^\infty \epsilon^3 d\epsilon \int_{-1}^1 \mu d\mu \; f_n(r\to\infty,\epsilon,\mu)}{\int_0^\infty \epsilon^2 d\epsilon \int_{-1}^1 \mu d\mu \; f_n(r\to\infty,\epsilon,\mu)} \,, \tag{23}$$

is plotted as a function of the scattering order n. After an initial small number of scatterings, $\langle\epsilon\rangle_n$ increases exponentially with scattering order (i.e., producing a straight line in Fig. 3), implying that the average fractional energy change per scattering, $\delta\epsilon/\epsilon$, remains constant and hence $\langle\epsilon\rangle_n \sim e^{(\delta\epsilon/\epsilon)n}$. The distribution, $f_n dn$, of the number of scatterings each photon experiences in a spherical flow depends on the details of the flow but often has an exponential tail, i.e., $f_n \sim e^{-\alpha n}$ for $n \gg 1$ (see, e.g., Sunyaev & Titarchuk 1980). As a result, the convolution of these two

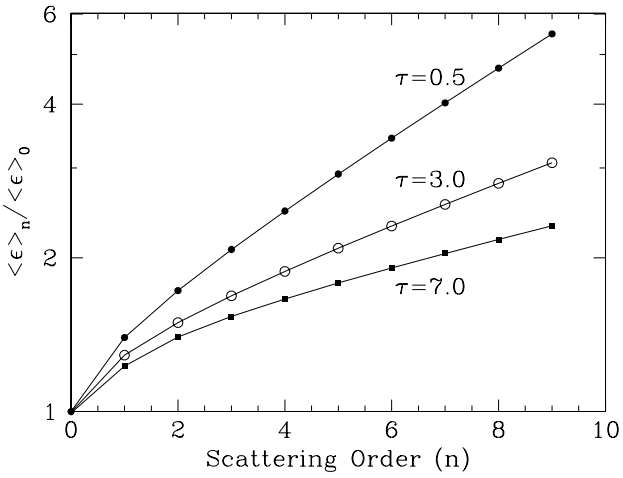

Figure 3. The average energy of photons emerging from the flows of Fig. 1 after a *given* number of scatterings. Results are shown for three representative optical depths. The photon energies are normalised to the average photon energy of photons that did not interact with the flow (which corresponds to the zeroth scattering order).

exponentials gives rise to the hard power-law spectrum of the form $f(\epsilon) \sim \epsilon^{-\alpha(\epsilon/\delta\epsilon)-1}$, as seen in Fig. 1. It is, therefore, the effect of multiple scatterings that produces the power-law spectra at high photon energies, for both low and high optical depths.

Note here that the average photon energy increases slower with scattering order for the flows with the larger total optical depth (see Fig. 3), a result that might appear at first counterintuitive. However, it can be understood as follows: the quantity $\langle\epsilon\rangle_n$ measures the average energy of photons that escape to infinity having experienced *only* n number of scatterings and not the average energy of all photons after each successive scattering. Indeed, when the total optical depth of the flow is low, photons that experience their $n-$th scattering very close to the inner boundary of the flow, and hence gain a lot of energy from the fast-moving electrons there, have a high chance of escaping to infinity and, consequently, contributing to $\langle\epsilon\rangle_n$. On the other hand, when the total optical depth of the flow is high, only photons that experience their $n-$th scattering away from the inner boundary of the flow, and hence gain a moderate amount of energy from scattering off slower electrons, escape to infinity and contribute to $\langle\epsilon\rangle_n$.

The emerging spectra at photon energies significantly larger than the injection energy correspond to photons that have been scattered by electrons a very large number of times and have therefore lost memory of their initial energy and angular distribution. For this reason, the slopes of the power-law tails depend only very weakly on the initial energy of the photons or the reference frame in which the boundary conditions are imposed. These examples (together with the discussion in Psaltis & Lamb 1997) demonstrate the similarity between the generation of power-law spectra tails in the flows considered here and in hot but static scattering media (Sunyaev & Titarchuk 1980).

Fig. 4 shows the optical depth dependence of the photon index, defined as the slope of the high-energy tail of the func-

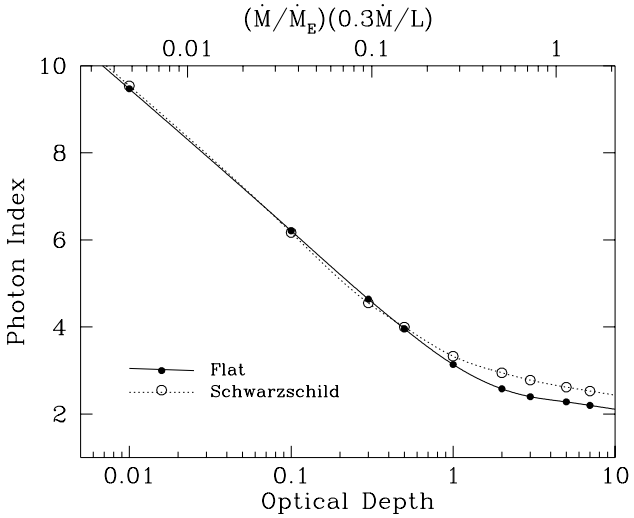

Figure 4. The optical depth dependence of the indices of the power-law tails generated by the flows shown in Fig. 1, as well as for the same flows but calculated for a flat spacetime. Note that the indices were calculated for the photon number spectra and not the energy spectra plotted in Fig. 1.

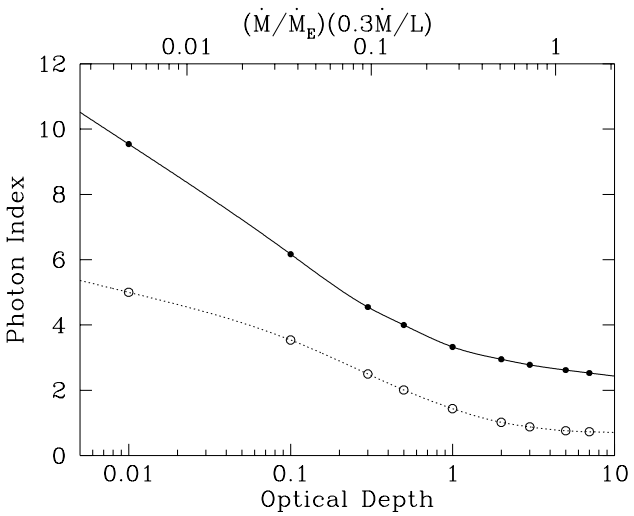

Figure 5. The optical depth dependence of the photon indices of the power-law tails generated by a free-falling medium onto a neutron star. The solid and dotted lines correspond to an absorptive and a semi-reflective inner boundary condition respectively, as described in the text.

tion $F(\epsilon)/\epsilon$ representing the photon number density. As was already obvious in Fig. 1, the power-law tails become flatter as the optical depth increases. Note here that the apparent saturation of the photon index at high optical depths is an artefact of our neglecting the systematic down-scattering of photons and the Klein–Nishina form of the scattering cross section. Taking these effects into account (which are of order $\epsilon/m_{\rm e}$ and higher) would produce, for high optical depths, a prominent Wien peak at energies comparable to the mean electron kinetic energy (Psaltis & Lamb 2000) and therefore affect the power-law nature of the emerging spectra. Moreover, at the corresponding high inferred accretion rates, the radial profiles of the electron density and velocity will not be the free-fall profiles assumed here.

Fig. 4 also demonstrates that for a free-falling medium and at high optical depths, the spectra calculated for a Schwarzschild spacetime are steeper than the ones calculated for a flat spacetime. This property can be traced back to the photon kinetic equation (12) and the effect on the emerging spectra of the terms of different orders in the electron bulk velocity β (see also discussion in Zampieri & Lamb 2000). Assuming a general electron velocity β, denoting the free-fall velocity as $\beta_{\rm ff}$, and expanding Eq. [12] up to second order in velocity, we obtain

$$\left\{\mu+\beta+\frac{1}{2}(\beta^2-\beta_{\rm ff}^2)\mu+\mathcal{O}[\beta(\beta^2-\beta_{\rm ff}^2)]\right\}\frac{df}{dr}=\frac{\eta}{\epsilon^3}-\chi f, \quad (24)$$

for a Schwarzschild geometry, and

$$\left[\mu+\beta+\frac{1}{2}\beta^2\mu+\mathcal{O}(\beta^3)\right]\frac{df}{dr}=\frac{\eta}{\epsilon^3}-\chi f\ , \quad (25)$$

for a flat geometry.

The generation of a power-law tail in the emerging spectrum is governed by the terms of order β^2 (Psaltis & Lamb 1997, 2000), which are the lowest order terms containing information about the kinetic energy of the electrons that can be transfered to the photons. Such terms appear both explicitly in Eqs. (24)–(25) and implicitly through the dependence of the characteristic curves, defined by Eqs. (13)–(14), on β^2; the latter contribution is negligible when the photon mean-free path is significantly smaller than any characteristic length-scale of the system. For a free-falling atmosphere in a Schwarzschild geometry, the explicit terms of order β^2 in the photon kinetic equation are identically cancelled by the terms of order $\beta_{\rm ff}^2$ that describe the gravitational redshift. Note, however, that the photons escaping to infinity have experienced –by definition– the last scattering in regions of very large photon mean-free path and, therefore, the cancellation of the systematic upscattering by general relativistic effects is not severe. As a result, the efficiency of the energy exchange between photons and fast moving electrons is reduced when general relativistic effects are taken into account and the effect is pronounced in flows with high optical depths, where a photon has suffered many scatterings before escaping.

As discussed above, the calculated photon indices are rather independent of the injection energy of the photons. However, they do depend strongly on the choice of the inner boundary condition for the flow. This is the case since the inner boundary condition affects the distribution of photon escape times from the flow and, hence, their average energy gain. Fig. 5 compares the results presented earlier with the power-law slopes of the spectra emerging from similar flows in which we have imposed a semi-reflecting inner boundary condition, i.e.,

$$f(r_{\rm in},\mu>0,\epsilon)=f(r_{\rm in},-\mu,\epsilon)+\frac{1}{\exp(\epsilon/T_{\rm b})-1}\ . \quad (26)$$

The spectra emerging from the flows with semi-reflecting boundaries are significantly flatter because the photons can be reflected a number of times between the flow and the inner boundary, gaining more energy, before emerging from the flow. The effect is very large, as the emerging spectrum can be very flat (index$\simeq$ 0.5) or steep (index$\simeq$ 2.5)

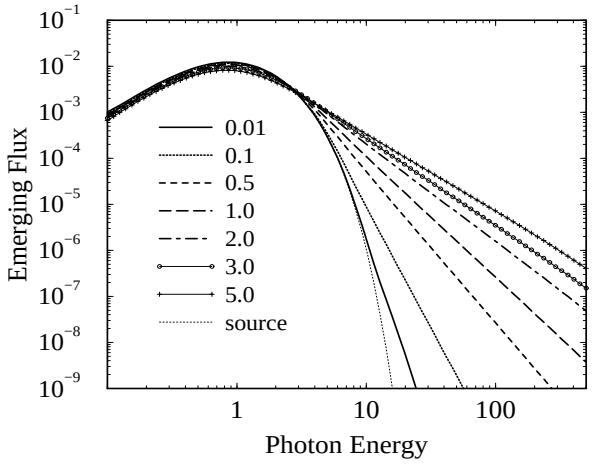

Figure 6. Radiation spectra emerging from scattering in radial accretion flows onto a black hole with different optical depths. The distribution of photon sources resembles the black-body emission from an underlying accretion disk (Eq. [15]). The emerging flux is in arbitrary units and the photon energy is in units of the temperature of the accretion disk at its inner boundary. The spectrum resulting in the absence of scattering (thin line) is also shown for comparison.

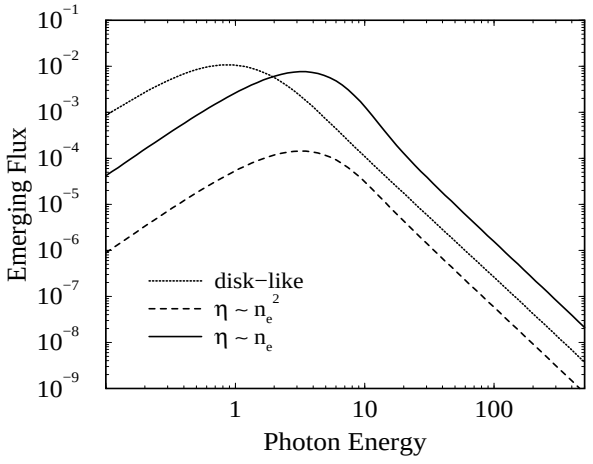

Figure 7. Radiation spectra emerging from radial accretion flows onto a black hole, with optical depth $\tau = 1$, but different emissivities (η) of soft photons (discussed in the text). The index of the power law at high energies is practically the same in all three cases.

for the same (large) value of the optical depth but for different boundary conditions.

5 RESULTS FOR BLACK HOLES

In this section we model the transport of photons in a radial accretion flow onto a black hole. In such a flow, the source of soft photons depends on the detailed properties of the accretion model and various simple expressions have been used so far in previous studies. Fig. 6 shows the spectra calculated for a disk-like source of photons (Eq. [15]), in a Schwarzschild spacetime, for different values of the optical depth (Eq. [16]). In order to demonstrate the effect of Comptonization on the spectral shape, the spectrum emerging from the flow in the absence of scattering has also been included. The resulting spectra consist of the soft source spectrum smoothly extending to a hard power law tail which becomes flatter with increasing optical depth, much like in flows illuminated from the surface of the neutron star presented in §4.

The power-law indices of the calculated spectra depend very weakly, if at all, on the radial distribution of the photon sources, as is evident in Fig. 7. This figure compares the spectra emerging from flows of optical depth $\tau = 1$ and for different expressions for the photon source: a disk-like source of photons (solid curve) and a volume emissivity that is proportional to the first (dashed curve) and second (dotted curve) power of the electron density. The close similarity of the power-law indices is yet another demonstration of the fact that the spectral tails result from multiple scatterings of photons by electrons which erase all memory of initial photon distributions (see also discussion in §4).

Even though the basic mechanism for the generation of the power-law spectral tails is the same for a flow around both a neutron star and a black hole, these systems differ in two respects: the location of the inner boundary and its radiative behaviour. The former brings out both the dramatic effect of the curvature of the spacetime and the extreme velocities, while the latter excludes the central object from any radiative contributions.

In an accretion flow around a black hole, the inner boundary lies at the event horizon, in the vicinity of which the free-fall velocity approaches the speed of light. Photons that propagate near the event horizon are dragged inwards by the converging flow, even in the presence of intense scattering that would tend to enhance their diffusion outwards. Moreover, among photons with small impact parameters (i.e., $b \leq 3\sqrt{3}/2$), only those directed almost radially outwards can escape the steep potential. The effects of the velocity field and the spacetime geometry on the fraction of photons that can escape to infinity from a distance r from the centre of the source are disentangled in Fig. 8. For illustration, given an isotropic source of photons located at radius r, the fraction of escaping photons is calculated at the free streaming limit, and corresponds to the fractional solid angle subtended by the characteristics that reach radial infinity. The combination of the effects of velocity and geometry, in the self-consistent picture of free falling material in a Schwarzschild spacetime, causes a steep photon deficiency inwards of $r = 1.5$, where trapped photon trajectories exist. From Fig. 8, it is evident that the properties of the flow and of the spacetime inside $r = 1.5$ affect very little the radiation that reaches the observer. This would not be true if our description ignored the curved geometry of the spacetime.

The other distinctive difference between a black hole and a neutron star is the radiative behaviour of the inner boundary (which, in the case of a neutron star, affects strongly the emerging spectrum as discussed in §4). The inner boundary in the case of a black hole is its event horizon, out of which no radiation can escape. In order to isolate the effect of the location of the inner boundary from that of the type of the inner boundary condition (i.e., the radiative behaviour of the boundary), we performed a set of calculations

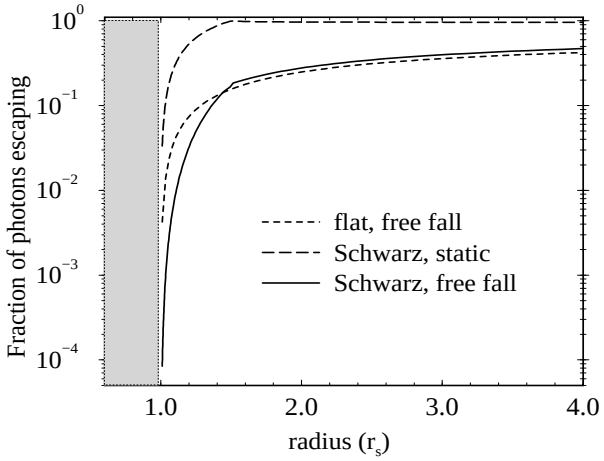

Figure 8. The fraction of photons emitted by an isotropic source of radiation at radius r that escape to infinity, for combinations of different spacetime geometries and velocity fields.

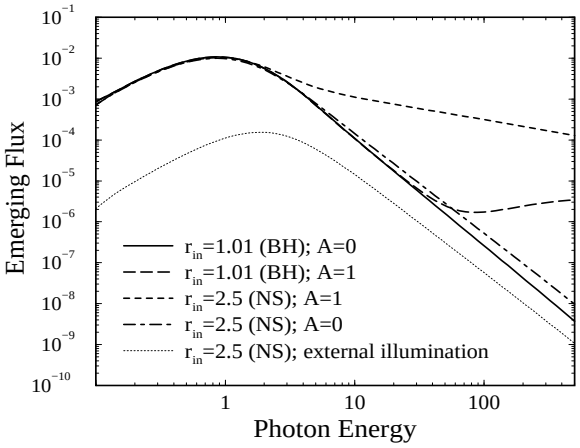

Figure 9. Radiation spectra emerging from radial accretion flows with the same optical depth $\tau = 1$ but different locations and radiative behaviours of the inner boundary. BH stands for a boundary appropriate for a black hole, while NS stands for neutron star. $A = 0$ ($A = 1$) corresponds to a fully absorptive (reflective) inner boundary. The case of external illumination with no photon sources within the flow is also shown for comparison.

with all possible combinations of the two, some of which are unphysical.

The results of the calculations, in which we vary the location and behaviour of the inner boundary condition but keep the optical depth of the scattering medium ($\tau = 1$) and the functional form of the photon sources (disk-like; see Eq. 15) fixed, are presented in Fig. 9. We use the albedo (A) to refer to the radiative behaviour of the inner boundary condition. The flattest spectrum (short-dashed curve) corresponds to a configuration that is realistic for a neutron star, with $r_{\rm in} = 2.5$ and a totally reflective inner boundary condition, i.e., $A = 1$. The dot-dashed curve shows the spectrum of a hypothetical neutron star that absorbs all radiation that hits its surface without reemiting any of it ($A = 0$). The range between these two curves is covered by similar flows of intermediate albedoes. The steeper spectrum in the latter case is caused by the relative deficiency of photons available for upscattering (see Fig. 5 and its discussion in §4). Accordingly, the spectrum resulting from a similar flow onto a black hole (solid curve) is steep but not considerably more so. The enhanced energy gain by the photons due to the much higher velocities encountered closer to the event horizon is compensated for by the shielding of the immediate neighbourhood of the horizon by the combined effect of curvature and free-fall velocity (demonstrated in Fig. 8). The long-dashed curve corresponds to a flow that reaches the horizon with a reflective inner boundary condition. This is certainly an unphysical configuration; it is nevertheless instructive. The resulting spectrum coincides with that of the black hole with an absorptive inner boundary condition, apart from a turnover at the hardest end which is, however, totally artificial. As we have already discussed in §2, due to the coordinate singularity at the horizon, the inner boundary is placed *very close to*, but not *at* the horizon. The radiation that is reflected off this inner boundary shows as the hard excess. A choice of an inner boundary closer to the horizon (which can be achieved at a low computational cost with our logarithmic grid in $r - 1$) pushes this artificial excess to higher photon energies. Apart from this artefact of the numerical method, it is evident that the particular form of the inner boundary condition, for the case of accretion onto a black hole, does not affect the emerging spectrum. Indeed, the absorptive character of the inner boundary is equivalent to the coincidence of this boundary with the black hole event horizon, since the propagation of the photons in its vicinity is determined entirely by the properties of the spacetime.

We turn now to examine the effect of neglecting the curvature of the spacetime (as has been done in a large number of previous studies, see discussion in §1) for the case of a flow that reaches the event horizon of a black hole. In Fig. 10, we present the results of calculations using the Schwarzschild metric (thick lines) or a flat spacetime geometry (thin lines). We performed both calculations for disk-like photon sources (Eq. [15]) and for an optical depth of $\tau = 3$. The radial distribution of the flux is shown for three representative observed photon energies: one around the peak of the local emissivity function (3 $T_{\rm in}$ in this case), one below the peak (0.3 $T_{\rm in}$) and one at the hard spectral tail (300 $T_{\rm in}$). There is no substantial difference in the amount of soft radiation reaching the observer between the calculations performed for the two different spacetime geometries. This is true because the flux at a certain radius and at frequencies around or below the spectral peak mainly correspond to photons that have not experienced any scattering with electrons. The hard spectral tail, though, which is the result of multiple upscatterings, is significantly different between the two calculations. Since no trapped photon characteristics exist in flat geometry (see §3), a larger fraction of photons from radii close to the event horizon can escape and thus provide copious numbers of photons to be further upscattered. This effect compliments the one already discussed in §4, i.e., that general relativistic effects reduce the efficiency of bulk Comptonization, identically cancelling it in the limit of very small photon mean-free path. The net result is again a flatter power-law spectrum for the calculation in a flat spacetime. This is qualitatively the same as for the case of accretion onto a neutron star

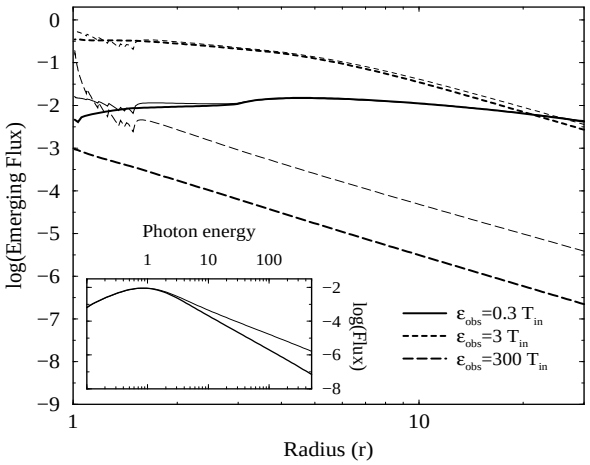

Figure 10. Radial profiles of flux at three representative observed photon energies: one below the peak of the local emissivity (0.3 $T_{\rm in}$), one around its peak (3 $T_{\rm in}$), and one at the hard tail (300 $T_{\rm in}$). Comparison between the results in a Schwarzschild (thick curves) and flat (thin curves) spacetime. The observed spectrum for the two cases is shown in the insert.

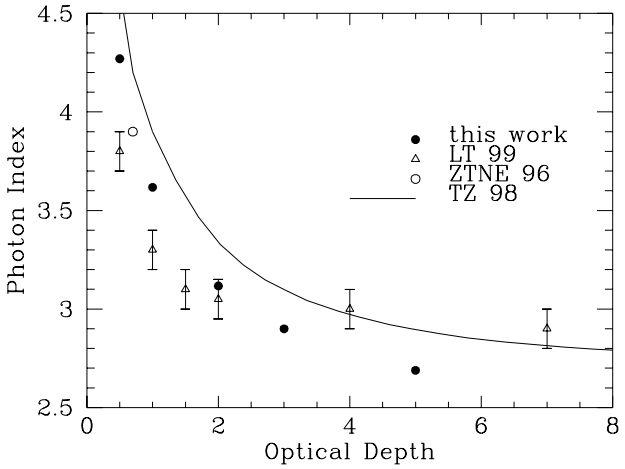

Figure 11. Comparison between different studies of the photon indices calculated for bulk Comptonized spectra from spherically accreting flows onto a black hole as a function of optical depth. The results of this work correspond to the spectra shown in Fig 6. Comparisons are done with the cold-flow solution of Zane et al. (1996; ZTNE 96), the analytic calculation of Titarchuk & Zannias (1998; TZ 98), and the zero-temperature Monte-Carlo solutions of Laurent & Titarchuk (1999; LT 99). The points in the latter case correspond to accretion flows with the same electron density profile as the current calculations (note the difference in our definition of optical depth) and the error bars represent the quoted 5% uncertainty in the fitted power-law indices.

(see §4) but more pronounced, as expected. For the cases shown in Fig. 10, the photon index is $\simeq 2.45$ for the flat and $\simeq 3.03$ for the Schwarzschild spacetime (compare with the difference of photon spectral indices in the case of a neutron star shown in Fig. 4).

Finally, Fig. 11 compares our results to previous calculations in which the effects of general relativity were explicitly taken into account. The photon index values we have obtained are consistent with the single case of cold, radial accretion onto a black hole studied by Zane et al. (1996) and similar to the Monte Carlo solutions of Laurent & Titarchuk (1999) for low optical depths. At high optical depths, our solutions correspond to slightly flatter spectra than those of Laurent & Titarchuk (1999) and the difference can be attributed to two effects: First, we neglected the systematic down-scattering of photons as well as the Klein–Nishina corrections to the scattering cross section, both of which tend to reduce the efficiency of energy exchange and hence produce steeper spectra. Second, the accretion flows in the calculations of Laurent & Titarchuk (1999) are truncated at a radius smaller than in our calculations (i.e., at $r_{\rm out} = 3$) and therefore the energy gained by the interaction of photons with electrons at larger radii is not taken into account. Finally, it is unclear how to compare our results to the analytic solutions of Titarchuk & Zannias (1998), who calculated the eigenfunctions of the transfer equation for flows with neither external illumination (Eq. [24]) nor photon sources within the flow (Eq. [16]).

6 CONCLUSIONS

We have solved the radiative transfer equation that describes scattering of photons by cold electrons moving at relativistic speeds, in steady-state, spherically symmetric accretion flows onto neutron stars and black holes. We used an iterative procedure to integrate the radiative transfer equation along the photon characteristics. This is an efficient method that allows for the full description of the spacetime geometry and the velocity field (see Schmid–Burgk 1978 and Zane et al. 1996), independent of the optical thickness of the flow. In this paper, we focused on examining simple configurations with the intention of exploring the generation of hard power-law spectra from accretion flows. We have examined the dependence of the resulting spectra on the boundary conditions, the properties of the scattering medium, and the approximations often used for the spacetime geometry and the velocity field.

We demonstrated that the generation of power-law spectral tails is the result of multiple scatterings of the soft source photons by the fast moving cold electrons (see also Laurent & Titarchuk 1999), at both low and high optical depths. As a result, the photons emerging from the accretion flow with high energies do not carry any signatures of regions of high electron velocities or spacetime curvature - contrary to expectations- but rather reflect the fact that a small number of photons can experience a significant number of scatterings even in a flow of small total optical depth. This mechanism is very similar to the generation of power-law spectra by thermal Comptonization in static media. It differs, however, from the generation of power-law spectra by non-thermal electrons in optically thin media, which is the result of a single scattering by a power-law distribution of relativistic electrons (see Coppi 1999).

The multiple scatterings experienced by the photons tend to wipe out all memory of initial conditions such as the radial, angular, or energy distribution of the sources. However, the resulting spectra for *neutron-star* flows do depend sensitively on the choice of the inner boundary conditions, confirming results reported earlier (Titarchuk et al. 1997,

Psaltis 1998; Psaltis & Lamb 2000). It is important to note, nevertheless, that none of the idealised boundary conditions used in our calculations is, strictly speaking, astrophysically relevant for a radial accretion flow onto a neutron star. Indeed, whether the photons that reach the inner boundary will be absorbed or reflected depends on the photon energy and the ionization state of the surface layers of the neutron star. Even if most of the photons are reflected, their energy gain at reflection will be determined by the thermal state and stratification of the transition region between the flow and the stellar surface. Moreover, the presence of shocks at this interface introduces additional complications. As a result, the spectral signature of a nearly-radial accretion flow onto a neutron star will not be uniquely determined by the flow properties but will be dictated by the specifics of the interaction of the flow with the stellar surface.

On the contrary, the spectral indices of the hard spectral tails resulting from the same flows onto black holes are immune to the inner boundary condition. This is due to the physical character of the inner boundary (the event horizon), i.e., that no radiation can escape to infinity (see Fig. 8 & 9). For this reason, the spectra produced from bulk Comptonization in a *purely radial, free-falling* flow onto a black hole have a power law index that is determined *solely* by the optical depth (or mass accretion rate Eq. [18]; see also discussion in Titarchuk Zannias 1998). Furthermore, when compared to the spectral tails from flows onto neutron stars in this idealised limit, those of black holes are steeper.

Several previous studies have examined the generation of power-law spectra without taking into account the curvature of the spacetime or the regime of highly relativistic speeds (e.g., Payne & Blandford 1981; Titarchuk et al. 1987; Psaltis & Lamb 2000). We showed that, for a free-fall velocity profile, general relativistic effects identically cancel the bulk Comptonization effects *everywhere* in the flow, including radii very far from the compact object, as long as the photon mean-free path is very small. If this were not true, then an observer comoving with the flow would be able to distinguish between being at rest at infinity and free-falling onto the compact object by making only local (because of the small photon mean-free path requirement) measurements of the evolution of the photon spectrum with time. However, for typical accretion rates, nowhere in the flow is the photon mean-free path small. Moreover, the photons that escape to infinity have experienced their last scatterings in regions of large photon mean-free path. As a result, the aforementioned cancellation of $\mathcal{O}(\beta^2)$ terms reduces the Comptonization efficiency –with respect to the flat geometry case– only modestly in the case of flows onto neutron stars which are of relatively high optical depths. Ignoring the actual spacetime geometry, when modelling a flow onto a black hole, results in more severe over-predicting of the hard tail flux, though. For a black hole, the existence of trapped characteristics (see §3) deprives the outer parts of the flow from a large fraction of the photons that have reached close to the event horizon. Consequently, disregarding the Schwarzschild spacetime geometry can lead to overestimating the flux at high photon energies by more than an order of magnitude (e.g., at 100 $T_{\rm in}$ in the case of Fig. 10).

We thank Fred Lamb, Feryal Özel, Philipppos Papadopoulos, and Luca Zampieri for useful discussions and comments. This work was supported by a postdoctoral fellowship of the Italian MURST (H. P.), a postdoctoral fellowship of the Smithsonian Institution and also, in part, NASA (D. P.). We also thank MPI für Gravitationsphysik, Harvard-Smithsonian CfA, and University of Portsmouth (H. P.) as well as SISSA (D. P.) for their warm hospitality.

REFERENCES

Blandford R. D., Payne D. G., 1981, MNRAS, 194, 1033
Borozdin K., Revnivtsev M., Trudolyubov S., Shrader C., Titarchuk L., 1999, ApJ, 517, 367
Burrows A., Young T., Pinto P. A., Eastman R., Thompson T. A., 2000, ApJ, 539, 865
Chakrabarti S. K., Titarchuk L. G., 1995, ApJ, 455, 623
Coppi P., 1999, in Poutanen J. and Svensson R., ed., High Energy Processes in Accreting Black Holes, ASP Conf. Ser., 161, 375
Fryer C. L., Benz W., Herant M., 1996, ApJ, 460, 801
Grove J. E., Johnson W. N., Kroeger R. A., McNaron–Brown K., Skibo J. G., Philips B. F., 1998, ApJ, 500, 899
Laurent P., Titarchuk L., 1999, ApJ, 511, 289
Lazzati D., Ghisellini G., Celotti A., Rees M. J., 2000, ApJ, 529, L17
Lindquist R. W., 1966, Ann. Phys., 37, 487
Madau P., Thompson C., 2000, ApJ, 534, 239
Mastichiadis A., Kylafis N. D., 1992, ApJ, 384, 136
Mihalas D., 1978, Stellar Atmospheres. W. H. Freeman & Co., New York
Payne D. G., Blandford R. D., 1981, MNRAS, 196, 781
Psaltis D., 1998, PhD thesis, Univ. Illinois
Psaltis D., 2000, ApJ, submitted
Psaltis D., Lamb F. K., 1997, ApJ, 488, 881
———. 2000, ApJ, submitted
Rephaeli Y., 1995, ARA&A, 33, 541
Sazonov S. Y., Sunyaev R. 1998, ApJ, 508, 1
Schmid–Burgk J., 1978, Astr. Sp. Sc., 56, 191
Shakura N. I., Sunyaev R., 1973, A&A, 24, 337
Shrader C., Titarchuk L., 1998, ApJ, 499, L31
———. 1999, ApJ, 521, L121
Sikora M., Begelman M. C., Rees M. J., 1994, ApJ, 421, 153
Sunyaev R. A., Titarchuk L. G., 1980, A&A, 86, 121
Titarchuk L., Mastichiadis A., Kylafis N. D., 1997, ApJ, 487, 834
Titarchuk L., Zannias T., 1998, ApJ, 493, 863
Turolla R., Zane S., Zampieri L., Nobili L., 1996, MNRAS, 283, 881
Zampieri L., Lamb F. K., 2000, preprint
Zane S., Turolla R., Nobili L., Erna M., 1996, ApJ, 466, 871